HMSIW Cavity Filters Employing Various Complementary Split-Ring Resonators for Microwave Remote Sensing Applications

Lijun Wang [1,2,3], Zhengwei He [1], Yong Mao Huang [4], Shuai Ding [4], and Maurizio Bozzi [5]

[1] State Key Laboratory of Geohazard Prevention and Geoenvironment Protection
Chengdu University of Technology, Chengdu 610059, Sichuan, China
hzw@cdut.edu.cn

[2] College of Geophysics
Chengdu University of Technology, Chengdu 610059, Sichuan, China

[3] Chengdu College
University of Electronic Science and Technology of China, Chengdu 610051, Sichuan, China

[4] School of Physics
University of Electronic Science and Technology of China, Chengdu 611731, China
ymhuang128@gmail.com, uestcding@uestc.edu.cn

[5] Department of Electrical, Computers and Biomedical Engineering
University of Pavia, Pavia 27100, Italy
maurizio.bozzi@unipv.it.

Abstract ─ In this work, bandpass filters employing half-mode substrate integrated waveguide (HMSIW) cavities and various modified complementary split-ring resonators (CSRRs) are presented. The two modified CSRRs, which are called as Type-I and Type-II CSRRs, can exhibit larger effective inductance and capacitance, and eventually to contribute to the size miniaturization of the resonators. Thereafter, as the two CSRRs are independently loaded into HMSIW cavities, the newly-formed HMSIW-CSRR cavity resonators can achieve more size reduction as compared with the HMSIW cavity with the conventional CSRR. To demonstrate the proposed concept, two HMSIW cavity bandpass filters independently loaded with the proposed Type-I and Type-II CSRRs are implemented. Experimental results shows that measurements of the proposed filters agree with their corresponding simulations well. Meanwhile, as compared with some similar works, the two proposed filters achieve size reduction of 76.8% and 78.6%, respectively, as well as good selectivity, illustrating their suitability for the system integration application in microwave remote sensing and radar systems.

Index Terms ─ Bandpass filter, complementary split-ring resonator (CSRR), remote sensing system, substrate integrated waveguide (SIW).

I. INTRODUCTION

In contemporary wireless applications such as microwave remote sensing, mobile communications and radar systems, the radio frequency (RF) front-end is a fundamentally essential constituent for transmitting and receiving wireless signals. Generally, in a typical RF front-end of the microwave remote sensing system, bandpass filters are key components for frequency selection, which enable the remote sensing system to separate different channels or signals, and eventually realize sensing, detecting and controlling of different targets. More recently, with the rapid development of wireless technologies, many different operation modes and functions have been integrated in a single module. Nevertheless, integrating multiple functions together generally leads to larger physical size of the circuitry, which is inconvenient for practical applications. Under such situation, there is an increasing demand on the system integration that simultaneously focuses on the integration of circuit functions and the miniaturization of physical size.

On the other hand, substrate integrated waveguide (SIW) has captured plenty of attention in the past few years since it implements the planarization of the high-performance rectangular waveguide. Thanks to its quasi-closed form, SIW is with many merits like low loss, high

Submitted On: December 16, 2018
Accepted On: April 6, 2019

quality factor, and easy integration. Therefore, a large number of microwave components, including filters, have been developed [1]. Most reported SIW filters utilized the resonator-coupling scheme, that is, their typical unit cells are SIW cavity resonators, whose lengths and widths are generally about half guided-wavelength of the dominant mode in SIW. Thus, as operating at the same frequency, the conventional SIW cavity filters are usually larger than their corresponding microstrip counterparts in term of physical size, which consequently results in the SIW cavity filters being unsuitable for practical applications.

To improve the practicability of SIW cavity filters, various approaches for size miniaturization have been developed. The half-mode SIW (HMSIW) structure can help to reduce the size of SIW cavity by half or so [2]. The quarter-mode SIW (QMSIW) is an intrinsic resonant cavity and can get further size reduction of 50% on the basis of HMSIW cavity [3]. In [4], the defected ground structure (DGS) is etched on the surface of SIW to miniaturize the cavity size, and loading the SIW cavity with complementary split-ring resonator (CSRR) can even acquire more size reduction [5-7]. Another work introduces CSRR into QMSIW to achieve extra size miniaturization of 40% [8]. In [9], the C-shaped slots and microstrip stubs are simultaneously loaded into the circular SIW cavity to reduce its size by 80%. Recently, the stepped-impedance CSRR (SICSRR) has been proposed and utilized with HMSIW cavity for compact single- and dual-band filter applications [10, 11]. Additionally, the multilayered structure is utilized incorporating with the QMSIW and CSRRs for further size miniaturization [12]. However, the modification of CSRR hasn't been further investigated and applied deeply.

In this work, two different CSRRs, namely, Type-I and Type-II CSRRs, are developed and combined with HMSIW cavities to realize size-miniaturized bandpass filters. As compared with the conventional CSRR, the Type-I and Type-II CSRRs can exhibit larger effective inductance and capacitance, which makes them more preferred in size reduction applications. This work is organized as followed: Section II and III respectively investigate working principles of the two CSRRs and their application to size-miniaturized HMSIW cavity filters in detail. Experimental results of the two proposed filters, as well as their comparison with some similar state-of-art works, are briefly discussed in Section IV. Finally, a conclusion is given.

II. PROPOSED CSRRS AND HMSIW-CSRR CAVITIES

Figure 1 shows geometries and equivalent-circuit models of the conventional, Type-I and Type-II CSRRs. Here, L_r and C_r respectively stand for the equivalent inductance and capacitance of the conventional CSRR. L_1 and C_1 separately represent the extra equivalent inductance and capacitance contributed from the inner slots in Type-I CSRR. Similarly, in Type-II CSRR, L_2 and C_2 denote the incremental equivalent inductance and capacitance introduced by its inner-lengthened split, respectively. More exactly, equivalent-circuit models of the two proposed CSRRs can be clearly comprehended from their dual structures by applying duality. As is known, the dual structure of the conventional CSRR is the split-ring resonator (SRR) [13]. Hence, it can be simply obtained that the corresponding dual structures of the proposed Type-I and Type-II CSRRs are Type-I and Type-II SRRs, which have been given in Fig. 1 as well. By applying duality, the equivalent inductance and capacitance of the conventional CSRR can be derived from the equivalent capacitance and inductance of SRR. Specifically, as shown in Fig. 1 (a), the interrelation between the conventional single ring CSRR and SRR can be expressed as:

$$C_r = 4\varepsilon_0 L_{ro}/\mu_0, \tag{1}$$

$$L_r = \mu_0 C_{ro}/(4\varepsilon_0), \tag{2}$$

where L_{ro} and C_{ro} are the equivalent inductance and capacitance of the conventional SRR, respectively. μ_0 and ε_0 are the permeability and permittivity in free space.

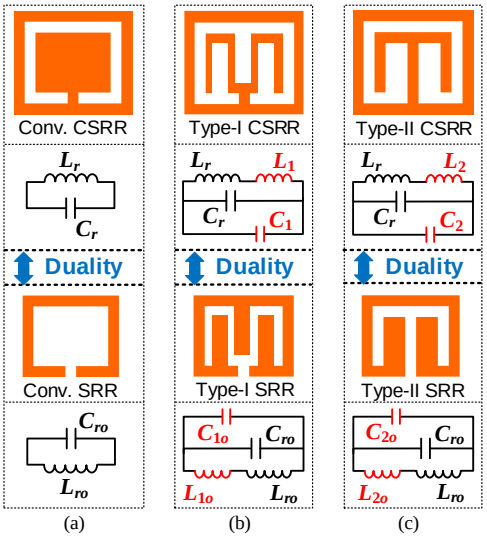

Fig. 1. Geometries and equivalent-circuit models of: (a) The conventional, (b) Type-I, and (c) Type-II CSRR.

Therefore, by using the duality theorem similarly, the equivalent inductance and capacitance of the Type-I and Type-II CSRRs can be derived from the equivalent capacitance and inductance of the Type-I and Type-II SRRs as well. For the proposed Type-I CSRR and its corresponding Type-I SRRs in Fig. 1 (b):

$$(C_1 + C_r) = 4\varepsilon_0 (L_{1o} + L_{ro})/\mu_0, \tag{3}$$

$$(L_1 + L_r) = \mu_0 (C_{1o} + C_{ro})/(4\varepsilon_0), \tag{4}$$

where L_{1o} and C_{1o} are the incremental equivalent

inductance and capacitance of Type-I SRR, respectively.

Similarly, for the proposed Type-II CSRR and its corresponding Type-II SRR in Fig. 1 (c):

$$(C_2 + C_r) = 4\varepsilon_0(L_{2o} + L_{ro})/\mu_0, \quad (5)$$

$$(L_2 + L_r) = \mu_0(C_{2o} + C_{ro})/(4\varepsilon_0), \quad (6)$$

where L_{2o} and C_{2o} are the incremental equivalent inductance and capacitance of Type-II SRR, respectively.

Then, resonant frequencies of the conventional, Type-I and Type-II CSRRs are respectively calculated as:

$$f_{\text{CSRR}} = 1\Big/\left(2\pi\cdot\sqrt{L_r\cdot C_r}\right), \quad (7)$$

$$f_{\text{T-I}} = 1\Big/\left[2\pi\cdot\sqrt{(C_r + C_1)\cdot(L_r + L_1)}\right], \quad (8)$$

$$f_{\text{T-II}} = 1\Big/\left[2\pi\cdot\sqrt{(C_r + C_2)\cdot(L_r + L_2)}\right]. \quad (9)$$

For the conventional, Type-I and Type-II SRRs, there are relations as: $(C_{1o}+C_{ro}) > C_{ro}$, $(L_{1o}+L_{ro}) > L_{ro}$, $(C_{2o}+C_{ro}) > C_{ro}$, and $(L_{2o}+L_{ro}) > L_{ro}$. Considering these relations with (4), (5) and (6) together, it can be captured that $(L_1+L_r) > L_r$, $(C_1+C_r) > C_r$, $(L_2+L_r) > L_r$, and $(C_2+C_r) > C_r$. Hence, as the conventional and proposed CSRRs are with the same outer physical size, dominate resonant frequencies of the proposed CSRRs will be lower than that of the conventional one. In other words, once the conventional, Type-I and Type-II CSRRs work at the same dominant frequency, outer sizes of the proposed ones will be smaller than that of the conventional one, which means physical size miniaturization is able to be expected. That is, the proposed CSRRs are electrically smaller than the conventional one as they operate at the same frequency. In addition, according to the geometry of Type-I SRR in Fig. 1 (b), the capacitance from inner stubs C_{1o} are dominant, while the inductance L_{1o} is smaller or even negative (a negative L_{1o} typically means L_{ro} and L_{1o} are parallel connected), which is mainly influenced by the specific geometrical dimensions. Therefore, for the Type-I CSRR, it can be deduced with the duality theorem that the inductance L_1 from the inner slots is dominant, while the capacitance C_1 is smaller or even negative (a negative C_1 typically means C_1 and C_r are series connected). On the other hand, according to the geometry of Type-II SRR in Fig. 1 (c), L_{2o} is mainly contributed from the inner-lengthening of the metal ring, and C_{2o} is mainly attributed from the widening of the split, which is originated from the lengthening of the metal ring. Hence, for the Type-II CSRR, it can be deduced with (9) that both C_2 and L_2 will have notable influence on the resonant frequency.

Subsequently, by etching the proposed CSRRs on the top metal cover of the HMSIW cavity, the Type-I and Type-II HMSIW-CSRR cavity resonators are formed, with their configurations listed in Fig. 2. With such defected electromagnetic structure being loaded on the top metal cover, the HMSIW cavity and the defected electromagnetic structure will interact with each other and further change distributions of the electromagnetic energy in the cavity. As a result, the evanescent mode resonance can be generated and size reduction of the HMSIW cavity will be eventually achieved [8].

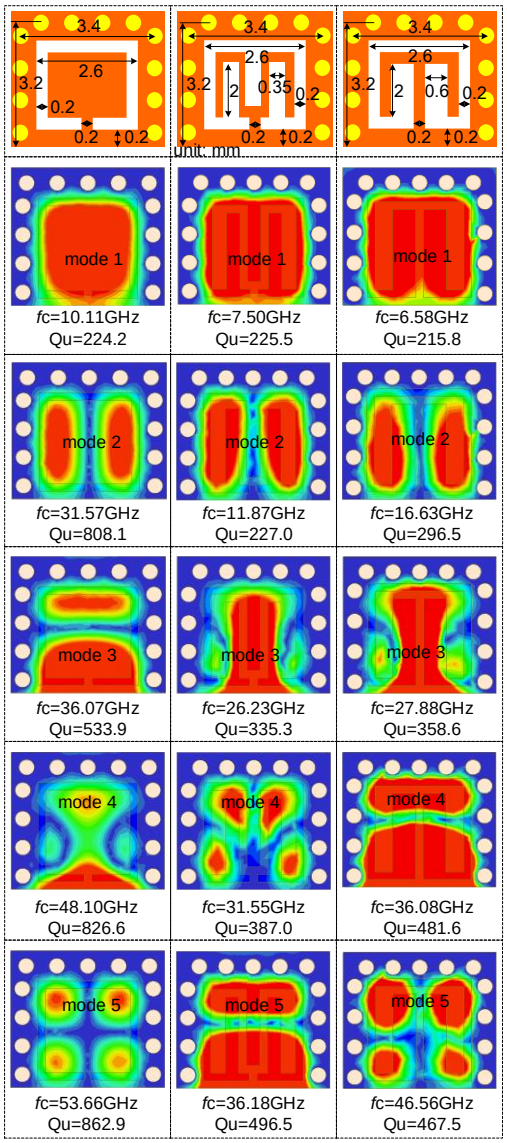

Fig. 2. Comparison of the simulated electric field distributions of the conventional, Type-I and Type-II HMSIW-CSRR cavity resonators.

Furthermore, since the proposed Type-I and Type-II CSRRs are more electrically compact than their corresponding conventional counterparts, they can help to acquire extra size reduction for the HMSIW cavity on the basis of the conventional CSRR [10,11]. In order to show the improvement in size reduction of the proposed Type-I and Type-II HMSIW-CSRR cavity resonators over the conventional one, some numerical simulations have been systematically carried out by using a commercial three-dimensional (3D) full-wave electromagnetic simulator. In order to study properties of these three cavities

conveniently and reasonably, all simulations are setup on a substrate with a relative permittivity of 2.94, a loss tangent of 0.0012, a thickness of 0.508mm, and a 0.035mm-thick conductor surface. For the full-wave electromagnetic simulator mentioned above, the PEC in its material library is with a conductivity of 1×10^{30}S/m, a relative permittivity of 1, and a relative permeability of 1, whereas the copper is with a default conductivity of 5.8×10^{7}S/m, a relative permeability of 0.999991, and a relative permittivity of 1. Hence, the PEC will contribute to better current conduction performance in the simulation, namely the simulated results with these two materials will be different, particularly on the conductor loss. Therefore, in the modeling setup, both the conductor surface and metallized vias are set as copper, instead of the perfect electric conductor (PEC), which is more accurate and realistic. Figure 2 shows comparison of the simulated electric field distributions of the conventional and the two proposed HMSIW-CSRR cavities, as well as their corresponding geometrical dimensions. It is clear that all the three HMSIW-CSRR cavities are with the same cavity size and slot-ring size, with the only difference on their splits. As shown in Fig. 2, the dominant resonant mode of the conventional HMSIW-CSRR cavity operates at 10.22GHz, while the proposed ones work at 7.5GHz and 6.58GHz, respectively. Hence, once the two proposed cavities are both set to operate at 10.22GHz, their physical sizes are supposed to be miniaturized. Meanwhile, the conventional HMSIW-CSRR cavity is with an unloaded quality factor (Q_u) of 224.2, whereas the proposed ones are with Q_u of 225.5 and 215.8, which means the three cavities in Fig. 2 are not with notable difference in term of the total loss. Actually, for these HMSIW-CSRR cavities, the radiation loss is dominate in the total loss.

Meanwhile, the lowest four higher-order modes in the conventional, Type-I and Type-II cavities are listed in Fig. 2 as well. Obviously, their first higher-order modes are the same one, mainly controlled by the CSRRs. On the other hand, their other three higher-order modes are much different with each other. For the conventional HMSIW-CSRR cavity, the operation frequency of its first higher-order mode is 31.57GHz, about three times of it's dominate resonant frequency. Whereas for the proposed cases, working frequencies of their first higher-order modes are 11.87GHz and 16.63GHz, respectively, about 1.58 and 2.53 times of their dominate operation frequencies. Moreover, resonate frequencies of the second, third and fourth higher-order modes of the proposed HMSIW-CSRR cavities are also much lower than the corresponding counterparts of the conventional one. It is clear that such difference is mainly caused by the difference between the conventional and proposed CSRRs.

III. HMSIW-CSRR CAVITIES FILTERS

To verify the aforementioned idea, two bandpass filters made of the proposed HMSIW-CSRR cavity resonators in Fig. 2 are developed. Figure 3 gives detailed configuration of the proposed Type-I HMSIW-CSRR cavity filter. It is designed with a central frequency (f_c) of 8.5GHz, a fractional bandwidth (FBW) of 8%, and a ripple of in-band insertion loss of 0.1dB. Hence, the initiated inner coupling coefficients (k_i) and external quality factor (Q_e) of the proposed Type-I HMSIW-CSRR cavity filter can be calculated by using the elements of the Chebyshev lowpass prototype filter. For this case, the coupling coefficients matrix k and Q_e are:

$$k=\begin{bmatrix} 0 & 0.0735 & 0 \\ 0.0735 & 0 & 0.0735 \\ 0 & 0.0735 & 0 \end{bmatrix}, \tag{10}$$

$$Q_e = 12.893. \tag{11}$$

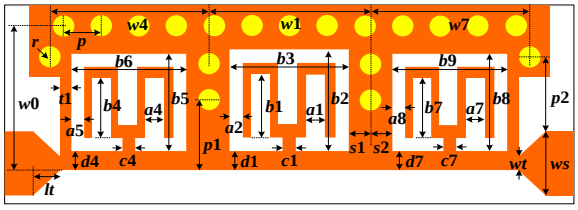

Fig. 3. Detailed configuration of the proposed Type-I HMSIW-CSRR cavity filter.

Afterwards, k_i and Q_e in the proposed Type-I HMSIW-CSRR cavity filter are numerically studied. These numerical simulations are carried out by using the same simulator mentioned above. Figure 4 sketches relation of the coupling window size between two adjacent Type-I HMSIW-CSRR cavity (px) and their k_i, with the scaled simulation model given in the inset. Figure 4 also shows the relation between width of the open port (pe) and Q_e, as well as the corresponding geometrical dimensions. Then, by taking Fig. 4 with (9) and (10) into consideration, the initiated geometrical parameters of the proposed Type-I filter can be selected. Finally, the entire filter in Fig. 3 is simulated and optimized by using the same full-wave simulator mentioned above.

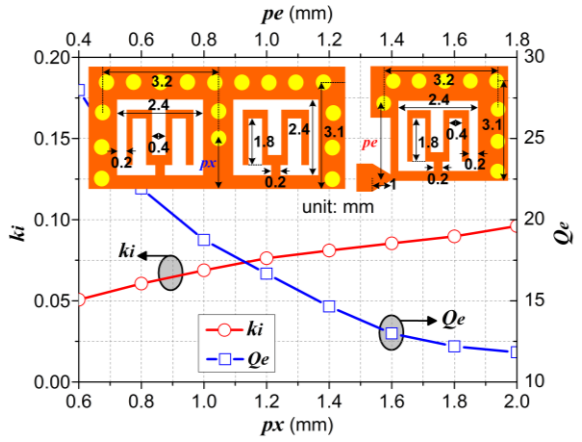

Fig. 4. Simulated k_i and Q_e in the proposed Type-I HMSIW-CSRR cavity filter.

Generally, there are two different strategies for the full-wave simulation and optimization. One is using the auto-optimization tool in the simulator, which can run optimizing procedures automatically. However, the auto-optimization typically cost too much time and not efficient in practical design. The second strategy is using the artificial tuning method. Firstly, setting initial values of geometrical parameters captured from the Eigenmode and coupling analyses as intermediate values. Then, choose two values for each geometrical parameter. For the two values, one is larger and the other is smaller than the intermediate one. Thirdly, by simulating the proposed filter respectively with geometrical dimensions of the larger, intermediate and smaller values, different results will be captured. Later, interrelation between the geometrical values and the transmission properties can be summarized by comparing these results. With the interrelation, it will be much faster to obtain the optimized values of the geometrical parameters of the proposed filter. For this case, some key geometrical parameters, including sizes of the cavities, widths of the coupling windows, and sizes of the feeding lines, are supposed to be tuned and simulated firstly, so that the optimization can be more efficiently. The optimized geometrical parameters are: lt=0.50, wt=0.25, ws=1.25, $w0$=3.10, $w1$=3.25, $w4$=$w7$=3.20, $s1$=$s2$=0.40, $t1$=0.20, r=0.20, p=0.70, $p1$=1.30, $p2$=1.55, $a1$=0.30, $a2$=0.20, b1=1.60, $b2$=$b3$=2.40, $c1$=0.20, $d1$=0.20, $a4$=0.30, $a5$=0.20, $b4$=1.60, b5=b6=2.40, $c4$=0.20, $d4$=0.20, $a7$=0.30, $a8$=0.20, b7=1.60, $b8$=$b9$=2.40, $c7$=0.20, $d7$=0.20 (unit: mm).

Later, for the proposed Type-II HMSIW-CSRR cavity filter in Fig. 5, it also contains three basic resonators and designed with the same specifications as the Type-I one. Naturally, same design procedures mentioned above are utilized to the Type-II filter as well. Figure 6 shows relation between width of the coupling window (px) and k_i of two adjacent Type-II HMSIW-CSRR cavities, and relation between width of the open port (pe) and Q_e, with the scaled simulation model simultaneously shown in the inset. Finally, the proposed Type-II HMSIW-CSRR cavity filter is simulated, with the optimized geometrical parameters as below: lt=0.50, wt=0.25, ws=1.25, $w0$=2.80, $w1$=3.00, $w4$=$w7$=2.95, $s1$=$s2$=0.40, $t1$=0.20, r=0.20, p=0.70, $p1$=1.20, $p2$=1.45, $a1$=0.50, $a2$=0.20, $b1$=1.29, $b2$=$b3$=2.20, $c1$=0.20, $d1$=0.20, $a4$=0.40, $a5$=0.20, $b4$=1.35, $b5$=$b6$=2.15, $c4$=0.20, $d4$=0.20, $a7$=0.40, $a8$=0.20, $b7$=1.35, $b8$=$b9$=2.15, $c7$=0.20, $d7$=0.20 (unit: mm). And the artificial tuning method is utilized again in the simulation and optimization as well.

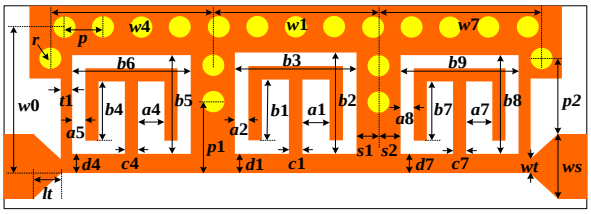

Fig. 5. Detailed configuration of the proposed Type-II HMSIW-CSRR cavity filter.

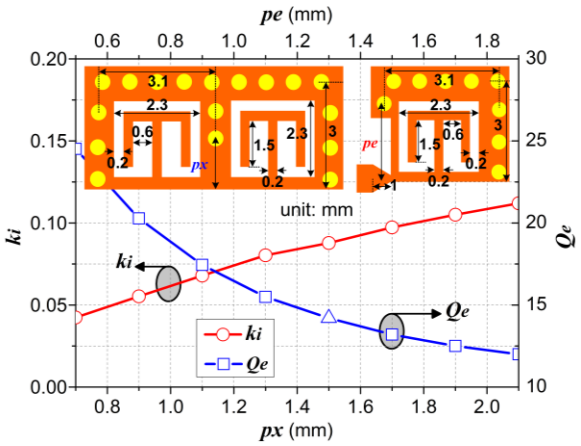

Fig. 6. Simulated k_i and Q_e in the proposed Type-II HMSIW-CSRR cavity filter.

IV. EXPERIMENTAL RESULTS

Prototypes of the proposed Type-I and Type-II HMSIW-CSRR cavity filters are fabricated by using the standard printed circuit board (PCB) process on a Rogers RT/Duriod 6002 substrate, with a thickness of 0.508mm, a relative permittivity of 2.2±0.02, a loss tangent of 0.0012. In the fabrication, the surface copper is grown with extra thickness of 0.011mm on the basis of the original copper of 0.024mm. Moreover, the metallized via-holes and the defected surface copper are dealt with separately: The via-holes are drilled firstly, with the mask corrosion and surface gold metal electroplating subsequently. Finally, all the via-holes are metallized by

wet electroplating. Photograph of the two fabricated HMSIW-CSRR cavity filter is given in the inset of Fig. 7 and Fig. 8, respectively. It can be easily captured that the functional part of the fabricated Type-I HMSIW-CSRR cavity filter is with a size of 3.9mm×10.0mm, while the value is 3.8mm×9.5mm for the Type-II case.

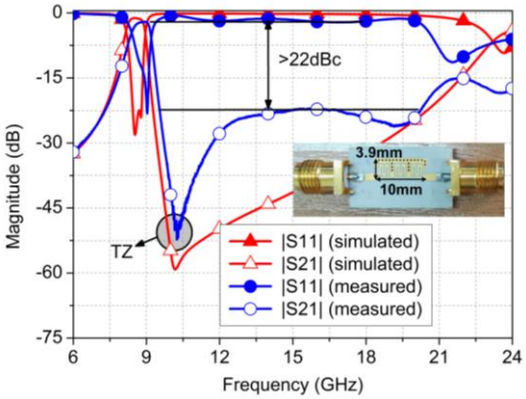

Fig. 7. Simulated and measured |S21| and |S11| of the fabricated Type-I HMSIW-CSRR cavity filter.

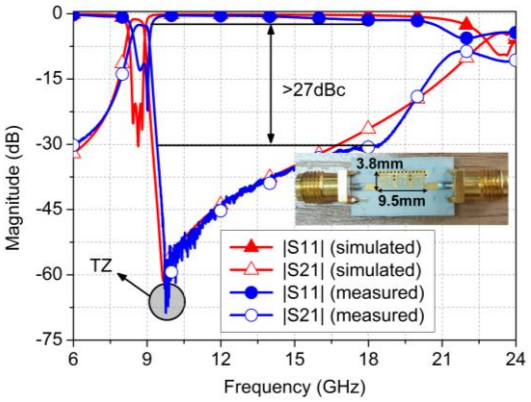

Fig. 8. Simulated and measured |S21| and |S11| of the fabricated Type-II HMSIW-CSRR cavity filter.

The fabricated HMSIW-CSRR cavity filters are measured by using a Keysight vector network analyzer N5242A, with the default SOLT calibration being used. Figure 7 shows measured and simulated magnitude of the transmission coefficient (|S21|) and input reflection coefficient (|S11|) of the fabricated Type-I filter. The fabricated Type-I filter achieves an f_c of 8.56GHz, a FBW of 7.8%, an in-band insertion loss of 1.62dB, and an in-band return loss better than 15dB. A transmission zero (TZ) located at 10.3GHz is able to provide suppression over 50dB, with the stopband up to 20GHz with rejection over 22dBc. On the other hand, measured and simulated results of the fabricated Type-II filter are given in Fig. 8. It can be obtained that the fabricated Type-II filter can exhibit an f_c of 8.60GHz, a FBW of 7.1%, an in-band insertion loss of 2.05dB, and an in-band return loss better than 13dB. Moreover, a TZ is captured at 9.7GHz with the rejection over 70dB, and the relative out-of-band suppression is larger than 27dBc from 9.2GHz to 18GHz.

In addition, Table 1 lists the comparison between the proposed HMSIW-CSRR cavity filters and some reported state-of-art works in similar technologies. Here, ε_r denotes the relative permittivity of the substrate. According to Table 1, as compared with the filter using QMSIW cavity and coplanar waveguide (CPW) resonator in [3], the filter employing SIW cavity and DGS in [6], and the filter utilizing SIW, C-shaped slots and microstrip stubs in [9], the proposed HMSIW-CSRR cavity filters are with much smaller electrical size. Particularly, as compared with the filter in [7], the proposed Type-I and Type-II filters separately achieve size reduction over 76.8% and 78.6%. Therefore, the two proposed HMSIW-CSRR cavity filters have the smallest size, as well as good performance.

Table 1: Comparison between some similar SIW cavity filters and the proposed HMSIW-CSRR cavity filters

Ref.	Poles	Topology	f_c (GHz), FBW	Elec. Size ($\lambda_0^2/\varepsilon_r$)
[3]	3	QMSIW+CPW	4.00, 16%	0.431
[6]	3	SIW cavity+DGS	4.90, 9.2%	0.406
[9]	3	SIW+slot+stub	5.20, 6.3%	0.410
I	3	HMSIW cavity+ Type-I CSRR	8.56, 7.8%	0.094
II	3	HMSIW cavity+ Type-II CSRR	8.60, 7.1%	0.087

V. CONCLUSION

In this work, bandpass cavity filters based on the proposed Type-I and Type-II HMSIW-CSRR cavity resonators are designed, fabricated and measured. Compared with some reported similar works, the proposed HMSIW-CSRR cavity filters achieve notable size-reduction, both with amount over 76%, as well as good selectivity performance, which demonstrates that they are applicable for the system integration and packaging of microwave remote sensing systems.

ACKNOWLEDGMENT

This work was supported in part by the State Key Laboratory of Geohazard Prevention and Geoenvironment Protection Independent Research Project under Grant SKLGP2017Z005 and the Sichuan Science and Technology Program under Grant 2018GZ0518.

REFERENCES

[1] M. Bozzi, A. Georgiadis, and K. Wu, "Review of substrate-integrated waveguide circuits and antennas," *IET Microw. Antennas Propag.*, vol. 5,

no. 8, pp. 909-920, July 2011.

[2] Y. Wang, W. Hong, Y. Dong, B. Liu, H. J. Tang, J. Chen, X. Yin, and K. Wu, "Half mode substrate integrated waveguide (HMSIW) bandpass filter," *IEEE Microw. Wireless Compon. Lett.*, vol. 17, no. 4, pp. 265-267, Apr. 2007.

[3] S. Moscato, C. Tomassoni, M. Bozzi, and L. Perregrini, "Quarter-mode cavity filters in substrate integrated waveguide technology," *IEEE Trans. Microw. Theory Tech.*, vol. 64, no. 8, pp. 2538-2547, Aug. 2016.

[4] Y. L. Zhang, W. Hong, K. Wu , J. Chen, and H. J. Tang, "Novel substrate integrated waveguide cavity filter with defected ground structure," *IEEE Trans. Microw. Theory Tech.*, vol. 53, no. 4, pp. 1280-1287, Apr. 2005.

[5] Q. L. Zhang, W. Y. Yin, S. He, and L.-S. Wu, "Compact substrate integrated waveguide (SIW) bandpass filter with complementary split-ring resonators (CSRRs)," *IEEE Microw. Wireless Compon. Lett.*, vol. 20, no. 8, pp. 426-428, Aug. 2010.

[6] W. Shen, W. Y. Yin, and X. W. Sun, "Compact substrate integrated waveguide (SIW) filter with defected ground structure," *IEEE Microw. Wireless Compon. Lett.*, vol. 21, no. 2, pp. 83-85, Feb. 2011.

[7] W. Jiang, W. Shen, L. Zhou, and W. Y. Yin, "Miniaturized and high-selectivity substrate integrated waveguide (SIW) bandpass filter loaded by complementary split-ring resonators (CSRRs)," *J. Electromagn. Waves Appl.*, vol. 26, no. 11-12, pp. 1448-1459, Dec. 2012.

[8] D. E. Senior, A. Rahimi, and Y. K. Yoon, "A surface micromachined broadband millimeter-wave filter using quarter-mode substrate integrated waveguide loaded with complementary split-ring resonator," *IEEE MTT-S Int. Microw. Symp. Dig.*, Tampa, USA, pp. 1-4, May 2014.

[9] L. Riaz, U. Naeem, and M. F. Shafique, "Miniaturization of SIW cavity filters through stub loading," *IEEE Microw. Wireless Compon. Lett.*, vol. 26, no. 12, pp. 981-983, Dec. 2016.

[10] Y. M. Huang, Z. Shao, W. Jiang, T. Huang, and G. Wang, "Half-mode substrate integrated waveguide bandpass filter loaded with horizontal-asymmetrical stepped-impedance complementary split-ring resonators," *Electron. Lett.*, vol. 52, no. 12, pp. 1034-1036, June. 2016.

[11] Y. M. Huang, Y. Peng, Y. Zhou, H. Jin, S. Leng, and G. Wang, "Size-reduced dual-band HMSIW cavity filters loaded with double-sided SICSRRs," *Electron. Lett.*, vol. 53, no. 10, pp. 689-691, May 2017.

[12] Y. Z. Zhu, W. X. Xie, X. Deng, and Y. F. Zhang, "Compact modified quarter mode substrate integrated waveguide resonator and its application to filters design," *ACES Journal*, vol. 32, no. 2, pp. 163-166, Feb. 2018

[13] F. Martin, *Artificial Transmission Lines for RF and Microwave Applications*. Hoboken: Wiley, USA, 2015.

Lijun Wang is currently pursuing the Ph.D. degree at Chengdu University of Technology, Chengdu, China, and is also a Lecturer at Chengdu College of University of Electronic Science and Technology of China, Chengdu, China. Her research interests including data analysis and system implementation for remote sensing.

Zhengwei He received the Ph.D. degree from Chengdu University of Technology in 1998, where he is now a Professor and Dean of Institute of Geological Survey. His research interests including remote sensing, geographic information system and urban planning. He has authored and coauthored over 220 referred papers.

Yong Mao Huang received the Ph.D. degree from University of Electronic Science and Technology of China, Chengdu, China, in 2017. He has been an Assistant Professor with the Department of Information Engineering, Xihua University, Chengdu, China, from 2018. His research interests including substrate integrated circuits. He has authored and coauthored about 50 referred papers.

Shuai Ding received the Ph.D. degree from University of Electronic Science and Technology of China, Chengdu, China, in 2013, where he is now an Associate Professor. His research interests including the microwave circuits and computational electromagnetics. He has authored and coauthored over 80 referred papers.

Maurizio Bozzi received the Ph.D. degree from the University of Pavia (Italy) in 2000, where he is now an Associate Professor. His current research interests concern substrate integrated waveguide technology, computational electromagnetics and novel material for microwave circuit applications. He is a Fellow of the IEEE. He is an Elected Member of the Ad-Com of the IEEE Microwave Theory and Techniques Society. He has authored and coauthored over 400 referred papers.